Hollow waveguide photomixing for quantum cascade laser heterodyne spectro-radiometry

Damien Weidmann,[1,*] Brian J. Perrett,[2] Neil A. Macleod,[1] and R. Mike Jenkins[2]

[1]*Space Science & Technology Department, STFC Rutherford Appleton Laboratory, Harwell Science & Innovation Campus, Didcot, Oxfordshire OX11 0QX, UK*
[2]*QinetiQ, Malvern Technology Centre, St. Andrews Road, Malvern, Worcestershire WR14 3PS, UK*
**damien.weidmann@stfc.ac.uk*

Abstract: An integrated optic approach, using hollow waveguides, has been evaluated for a compact, rugged, high efficiency heterodyne optical mixing circuit in the middle infrared. The approach has involved the creation of hollow waveguides and alignment features for a beam combiner component in a glass-ceramic substrate. The performance of the integrated beam combiner was tested as part of a full laser heterodyne spectro-radiometer in which a quantum cascade laser local oscillator emitting at 9.7 μm was mixed with incoherent radiation. The performance has been evaluated with both cryogenically-cooled and peltier-cooled photomixers demonstrating consistent detection limits of two and five times the shot noise limit, respectively. The hollow waveguide mixer has also shown advantages in temporal stability, laser spatial mode cleansing, and reduced sensitivity to optical feedback.

OCIS codes: (300.6310) Spectroscopy, heterodyne; (140.5965) Semiconductor lasers, quantum cascade; (230.7370) Waveguides; (120.5630) Radiometry.

References and links

1. T. Kostiuk, T. A. Livengood, T. Hewagama, G. Sonnabend, K. E. Fast, K. Murakawa, A. T. Tokunaga, J. Annen, D. Buhl, and F. Schmulling, "Titan's stratospheric zonal wind, temperature, and ethane abundance a year prior to Huygens insertion," Geophys. Res. Lett. **32**(22), L22205 (2005).
2. K. Fast, T. Kostiuk, P. Romani, F. Espenak, T. Hewagama, A. Betz, R. Boreiko, and T. Livengood, "Temporal behavior of stratospheric ammonia abundance and temperature following the SL9 Impacts," Icarus **156**(2), 485–497 (2002).
3. G. Sonnabend, M. Sornig, P. J. Krotz, R. T. Schieder, and K. E. Fast, "High spatial resolution mapping of Mars mesospheric zonal winds by infrared heterodyne spectroscopy of CO2," Geophys. Res. Lett. **33**(18), L18201 (2006).
4. D. D. S. Hale, M. Bester, W. C. Danchi, W. Fitelson, S. Hoss, E. A. Lipman, J. D. Monnier, P. G. Tuthill, and C. H. Townes, "The Berkeley infrared spatial interferometer: a heterodyne stellar interferometer for the mid-infrared," Astrophys. J. **537**(2), 998–1012 (2000).
5. R. T. Menzies, "Laser heterodyne detection techniques", in Laser Monitoring of the Atmosphere, E. D. Hinkley, ed. (Springer, Berlin, 1976).
6. W. Bell, N. A. Martin, T. D. Gardiner, N. R. Swann, P. T. Woods, P. F. Fogal, and J. W. Waters, "Column measurements of stratospheric trace species over Are, Sweden in the winter of 1991-1992," Geophys. Res. Lett. **21**(13), 1347–1350 (1994).
7. R. T. Menzies, and R. K. Seals, Jr., "Ozone monitoring with an infrared heterodyne radiometer," Science **197**(4310), 1275–1277 (1977).
8. K. E. Fast, T. Kostiuk, F. Espenak, T. A. Livengood, T. Hewagama, and M. F. A'Hearn, "Stratospheric ozone profiles from Mauna Kea, Hawai'i (19.8°N, 155.5°W) using infrared heterodyne spectroscopy, 1988–2003," Geophys. Res. Lett. **31**(8), L08109 (2004).
9. D. Deming, F. Espenak, D. Jennings, T. Kostiuk, M. Mumma, and D. Zipoy, "Observations of the l0-μm natural laser emission from the mesospheres of Mars and Venus," Icarus **55**(3), 347–355 (1983).
10. D. A. Glenar, M. J. Mumma, T. Kostiuk, H. Huffman, J. Degnan, H. Dave, U. Hochuli, and P. Haldemann, "Miniaturized, 9-12 micron heterodyne spectrometer with space qualifiable design features," Proc. SPIE **1235**, 933–942 (1990).
11. G. Sonnabend, D. Wirtz, and R. Schieder, "Evaluation of quantum-cascade lasers as local oscillators for infrared heterodyne spectroscopy," Appl. Opt. **44**(33), 7170–7172 (2005).
12. D. Weidmann, W. J. Reburn, and K. M. Smith, "Ground-based prototype quantum cascade laser heterodyne radiometer for atmospheric studies," Rev. Sci. Instrum. **78**(7), 073107 (2007).

#143438 - $15.00 USD Received 1 Mar 2011; revised 6 Apr 2011; accepted 19 Apr 2011; published 25 Apr 2011

13. D. Weidmann, W. J. Reburn, and K. M. Smith, "Retrieval of atmospheric ozone profiles from an infrared quantum cascade laser heterodyne radiometer: results and analysis," Appl. Opt. **46**(29), 7162–7171 (2007).
14. G. Sonnabend, D. Wirtz, V. Vetterle, and R. Schieder, "High-resolution observations of Martian non-thermal CO2 emission near 10 μm with a new tuneable heterodyne receiver," Astron. Astrophys. **435**, 1181–1184 (2005).
15. D. Stupar, J. Krieg, P. Krötz, G. Sonnabend, M. Sornig, T. F. Giesen, and R. Schieder, "Fully reflective external-cavity setup for quantum-cascade lasers as a local oscillator in mid-infrared wavelength heterodyne spectroscopy," Appl. Opt. **47**(16), 2993–2997 (2008).
16. D. Weidmann, and G. Wysocki, "High-resolution broadband (>100 cm^{-1}) infrared heterodyne spectro-radiometry using an external cavity quantum cascade laser," Opt. Express **17**(1), 248–259 (2009).
17. R. L. Abrams, "Gigahertz tunable waveguide CO_2 laser," Appl. Phys. Lett. **25**(5), 304–306 (1974).
18. D. R. Hall, R. M. Jenkins, E. K. Gorton, and P. H. Cross, "A compact sealed waveguide CO_2 laser," J. Phys. D Appl. Phys. **10**(1), 1–6 (1977).
19. R. M. Jenkins, R. W. J. Devereux, and A. F. Blockley, "Hollow Waveguide Integrated Optics: a Novel Approach to 10.6 μm laser radar," J. Mod. Opt. **45**(8), 1613–1627 (1998).
20. R. M. Jenkins, R. Foord, A. Blockley, T. Papetti, D. Graham, and C. Ingram, "Hollow waveguide integrated optic subsystem for a 10.6-μm range-Doppler imaging lidar," Proc. SPIE **4034**, 108–113 (2000).
21. R. M. Jenkins, B. J. Perrett, M. E. McNie, E. D. Finlayson, R. R. Davies, J. Banerji, and A. R. Davies, "Hollow waveguide devices and systems," Proc. SPIE **7113**, 71130E, 71130E-8 (2008).
22. K. D. Laakmann, and W. H. Steier, "Waveguides: characteristic modes of hollow rectangular dielectric waveguides," Appl. Opt. **15**(5), 1334–1340 (1976).
23. J. F. Holmes, and B. J. Rask, "Optimum optical local-oscillator power levels for coherent detection with photodiodes," Appl. Opt. **34**(6), 927–933 (1995).
24. R. Schieder, and C. Kramer, "Optimization of heterodyne observations using Allan variance measurements," Astron. Astrophys. **373**(2), 746–756 (2001).

1. Introduction

Optical laser heterodyne spectro-radiometers (LHSR) operating in the middle infrared (mid-IR) combine high spectral resolution, high radiometric sensitivity and high spatial resolution. This makes them powerful tools for remote sounding in astronomy [1–4] and atmospheric applications [5,6]. In the 8-12 μm atmospheric window, where many molecules exhibit unique and strong ro-vibrational transitions, LHSR using CO_2 lasers as local oscillators (LO) have been used for ground-based atmospheric [7,8] and astronomical sensing [9]. Development of a system for space applications has also been considered [10]. However, a number of issues including the lack of laser frequency versatility, instrumental size, weight, and power requirements limit the practical applications of LHSR systems based upon gas laser sources. The advent of continuously tunable, solid state, quantum cascade lasers (QCL) operating in the mid-IR at room temperature, offers new prospects for the application of optical heterodyne instruments for atmospheric monitoring, astronomy, and space sciences. In this respect, QCL have been demonstrated as highly efficient LO in heterodyne spectro-radiometers [11]. This has led to the development of QCL-based heterodyne instruments [12] which have been demonstrated in both atmospheric and astronomical applications [13,14]. QCL-based LHSR with broadband tuning in the mid-IR (several tens of wavenumbers) were recently demonstrated using an external cavity configuration [15,16].

Further development of LHSR towards real world applications and deployment would be eased through the complete optical integration of the required active and passive system components in a single substrate. This prospect is investigated here. Optical integration can be achieved via the use of dielectric hollow waveguides (HW) which guide radiation through an optical circuit. Mid-IR HW were initially developed for CO_2 waveguide laser resonators [17,18] and are therefore particularly relevant for integration of a QCL-based instrument operating in the 8-12 μm range.

The use of HW to form complete integrated optical circuits, similar to those created with solid core waveguides, was first proposed and demonstrated in relation to a 10.6 μm coherent lidar system [19]. HW formed in the surface of a polycrystalline alumina substrate were used to guide light through a circuit of optical components, each being held in a precision alignment slot. The approach led to a compact, rugged lidar system, which exhibited very good coherent detection characteristics. Subsequently a Doppler anemometer with an integrated laser source and a range-Doppler imaging lidar [20] were demonstrated. More recently, the concept has been further developed for use at 1.55 μm [21]. The approach could be very beneficial for optical and laser based space instrumentation in minimizing size and

#143438 - $15.00 USD Received 1 Mar 2011; revised 6 Apr 2011; accepted 19 Apr 2011; published 25 Apr 2011

mass whilst simultaneously easing alignment tolerances and reducing sensitivity to vibration, shock and thermal effects in the harsh space environment.

A critical aspect of the performance of LHSR is the coherent mixing efficiency achieved when the LO is mixed with the incoming incoherent radiation to be analyzed. To evaluate the potential of a HW integrated optic approach to LHSR this paper focuses on the development of a simple HW mixer circuit and measurements of its performance characteristics. In the subsequent sections details of the work are presented in the following order: (i) the design and development of the HW mixer circuit, (ii) its integration with ancillary components to form a full QCL-based LHSR, (iii) the use of the LHSR to make laboratory measurements of the absorption and transmission spectra of carbonyl sulfide, (iv) comparative measurements of LHSR performance with a liquid nitrogen cooled photomixer and a Peltier cooled detector with an immersed lens, (v) conclusions and future work.

2. Hollow waveguide mixing circuit

The hollow waveguide mixing circuit is shown schematically in Fig. 1. It consists of two square section input waveguides (for the LO and received radiation), a beam combining optic and two output waveguides. As illustrated, the square section channels for the waveguides are formed in the substrate along with an alignment slot for the beam splitter component. A lid forms the upper wall of all the waveguides.

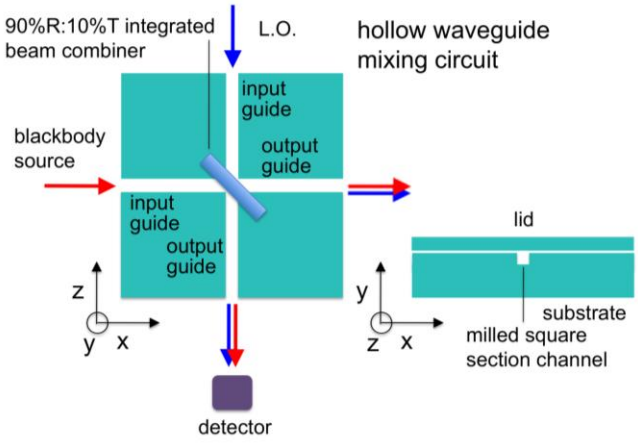

Fig. 1. Schematic of the hollow waveguide mixing circuit.

The waveguide mixing circuit was formed in a 10x10x1.5 cm^3 glass-ceramic (Macor) substrate. Square-sectioned channels (which form the basis of the HW) and precision alignment slots for integrated optical components, are machined into the substrate by computer numerically controlled (CNC) milling techniques. As illustrated in Fig. 1, a thin-film coated beam combiner, transmitting 10% of the LO power while reflecting 90% of the source radiation, is integrated into an alignment slot in the centre of the substrate.

2.1 Coupling

HW are intrinsically capable of supporting higher order modes in addition to the fundamental mode. Higher order modes are undesirable for LHSR because they are lossy and they reduce the efficiency of the heterodyne mixing efficiency [19]. However, in practice high fidelity fundamental mode excitation and propagation can be achieved and maintained in the HW mixer circuit under the condition that: (a) the waist dimension of the free-space TEM_{00} input field is optimized for fundamental mode excitation, (b) appropriate angular and lateral alignment tolerances are achieved between the free-space TEM_{00} input field and the input waveguide, and, for analogous reasons, (c) appropriate angular and lateral alignment

#143438 - $15.00 USD Received 1 Mar 2011; revised 6 Apr 2011; accepted 19 Apr 2011; published 25 Apr 2011

tolerances are achieved in coupling the fundamental mode field from one linear hollow waveguide in the circuit to another via an integrated transmission or reflective component.

These requirements are now considered in terms of interfacing the LO with the HW structure, starting with the need for efficient fundamental mode excitation. The transverse nature of the $EH_{mn}{}^{th}$ waveguide mode is defined by the two integers *m* and *n* in relation to the transverse axes of the waveguide *x* and *y*, respectively (see Fig. 1). For example, the fundamental mode is defined by *m = 1* and *n = 1*, the next highest order mode is defined by *m = 2* and *n = 1*. With respect to coupling a well aligned Hermite-Gaussian TEM_{00} beam into a square section hollow waveguide, Laakman and Steier [22] give the complex amplitude coupling coefficient, A_{mn} for the $EH_{mn}{}^{th}$ mode as:

$$A_{nm}(\omega_0) = C_n^x(\omega_0) \cdot C_m^y(\omega_0), \tag{1}$$

For a square section waveguide, the y and x components of the amplitude coupling coefficient have an identical form. For odd integers of *n*, the *x* component is given by:

$$C_n^x(\omega_0) = \left(\frac{2}{\pi}\right)^{1/4} \sqrt{\frac{\omega_0}{a}} \times \exp\left[-\left(\frac{n\pi\omega_0}{4a}\right)^2\right] \times RE\left[erf\left(\frac{4}{\omega_0}\right) - j\frac{n\pi}{4a} + c.c.\right]. \tag{2}$$

C_n^x is zero when *n* is even. It should be noted that $C_n^x(\omega_0)$ depends on a dimensionless parameter defined by the ratio of the radius of the beam waist ω_0 to the waveguide half width *a*. *RE()* denotes the real part, *erf()* the error function, *j* the standard imaginary unit and *c.c.* the complex conjugate. The power coupling coefficient is given by the square of the modulus of the complex amplitude coefficient, $|A_{mn}(\omega_0)|^2$.

Figure 2 shows calculations of the amplitude and power coupling coefficients for various waveguide modes as a function of the ratio ω_0/a. Optimizing the fundamental mode coupling is achieved when the ratio ω_0/a has fractional value of 0.703. This provides a fundamental mode power coupling coefficient of 0.979, i.e. ~98% of the power in the LO TEM00 beam is coupled to the fundamental mode of the hollow waveguide. Of the remainder ~1% of the power coupled into a range of higher order modes and a further ~1% lost due to aperturing at the guide entrance [21]. Use of this ratio of ω_0/a is the basis for the interfacing optics.

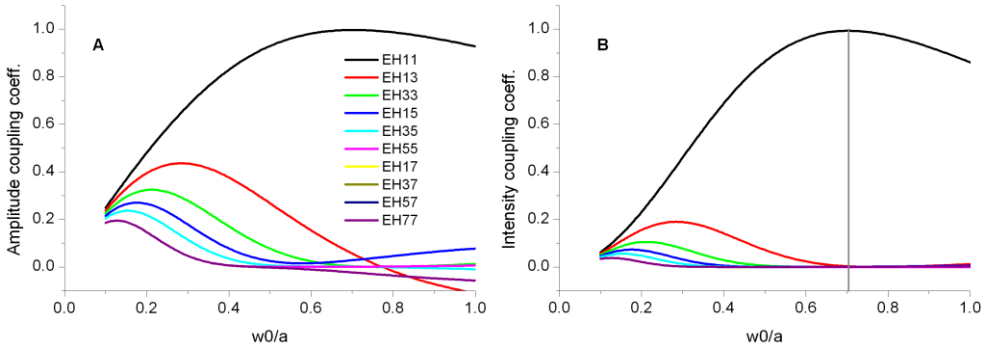

Fig. 2. A) Evolution of the amplitude and B) intensity coupling coefficients versus the dimension of the hollow waveguide for various Gaussian EH_{nm} waveguide spatial modes.

2.2. Design tolerances

Under the assumption that the optimum input beam radius has been achieved for maximizing the fundamental mode coupling, the angular and lateral alignment tolerances that are required at the input and in propagation through the hollow waveguide circuit and the components integrated within it, are considered next. The tolerance on angular alignment is proportional to the ratio of the wavelength to the guide width, whilst lateral alignment tolerance is directly proportional to the guide width [19,21]. Figure 3, illustrates calculations of the lateral and

#143438 - $15.00 USD Received 1 Mar 2011; revised 6 Apr 2011; accepted 19 Apr 2011; published 25 Apr 2011

angular alignment tolerances required to ensure > 95% fundamental mode power coupling. The tolerances are plotted as a function of guide width for an operational wavelength of 9.7 μm.

Based on the design curves in Fig. 3, a 1.0 mm^2 HW cross-section was chosen for the mixing circuit. This choice of guide cross-section dictates angular and lateral alignment tolerances of < 2.0 mrad and < 70 μm respectively, in order to ensure that high fidelity fundamental mode propagation characteristics are achieved in practice. In this respect, the largest source of angular misalignment in a HW circuit is due to the fit of the optical components into the alignment slots. The angular alignment achieved in practice is governed by the difference in thickness between any given integrated optical component and the associated alignment slot width/depth. Appropriate attention was paid to component metrology and the manufacturing process to ensure the required angular alignment tolerance was achieved. Separate calculations indicated that for a 1.0 mm^2 HW formed in Macor at an operational wavelength of 9.7 μm, the fundamental mode power transmission is > 95% for a 10 cm guide length [19]. This ensures very low optical power loss in propagation through the mixing circuit.

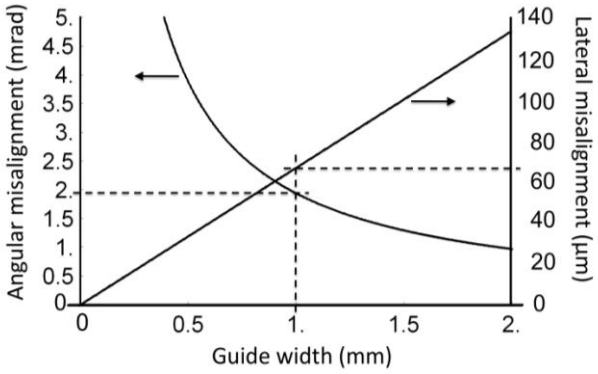

Fig. 3. Predictions of the trade-off between guide width and angular and lateral alignment tolerances for an operational wavelength of 9.7 μm.

3. Experimental details

A schematic of the full LHSR arrangement is shown in Fig. 4. The core of the setup consists of the HW mixing block to which four sub-modules are coupled, one per HW port. Coupling to the HW input ports is achieved via two off axis parabolic mirrors (OAPM) whose alignments were fixed using dowel pin techniques to provide alignment accuracies which meet the tolerances defined in section 2. Throughout the set up, with the exception of one aspheric lens, all optical elements are reflective to avoid chromaticity and limit the production of optical standing waves.

The HW mixing block has two outputs: the first, comprising 90% of the LO power, is dedicated to laser diagnostics, including power measurements, beam profiling, and frequency calibration. The second output, comprising 10% of the LO power, is imaged onto the heterodyne photomixer with a beam waist matched to the size of the detector element. Two photomixers are evaluated in this study: 1) a resonant optical cavity HgCdTe photodiode operating at liquid nitrogen (LN_2) temperatures (Raytheon Vision System), and, 2) an immersed lens HgCdZnTe photodiode operating with thermoelectric cooling (TEC). Both photomixers are electrically matched to biasing and amplifying circuits to achieve a high frequency cut off of 1 GHz. Radio-frequency pass-band filters can be connected to the photomixer output to modify the LHSR resolution and tailor the instrument lineshape. A Schottky diode detects the intermediate frequency RF power. The output of the Schottky diode is fed into a DSP lock-in amplifier for phase sensitive detection of the signal.

#143438 - $15.00 USD Received 1 Mar 2011; revised 6 Apr 2011; accepted 19 Apr 2011; published 25 Apr 2011

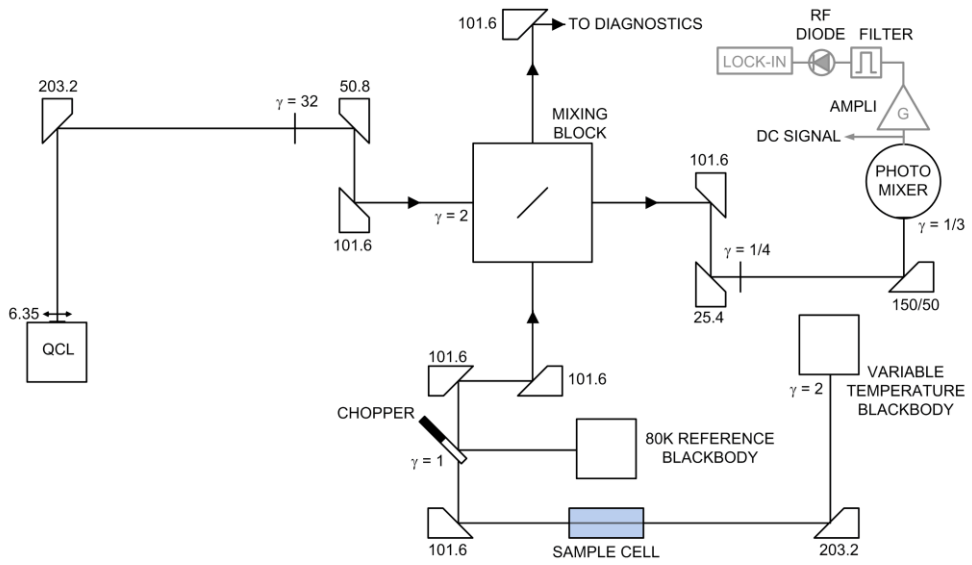

Fig. 4. Schematic of the optical setup implemented for the evaluation of hollow waveguide mixing for laser heterodyne spectro-radiometry. The numbers indicated by the optics corresponds to the focal lengths in millimeters. Magnification γ is indicated close to laser waist positions.

3.1 Quantum cascade laser coupling

As part of the LO input sub-module, a distributed feedback QCL operates continuous wave at – 30 to + 20°C with thermoelectric cooling. The laser threshold is 405 mA at 0°C with a maximum power of 30 mW at an injection current of 600 mA. The laser frequency is tuned using modulation of the injection current and/or temperature.

An anti-reflection coated aspheric Zinc Selenide lens (12.7mm diameter, 6.35mm back focal length) collimates the laser beam. After collimation, a group of three OAPM expands the beam waist size to match the fundamental mode coupling requirements of the HW port. Optics are aligned using a visible laser and remain fixed afterwards. The coupling optimization is made through adjustment of the laser position only.

The efficiency of the coupling was checked using an infrared micro-bolometer camera for far field measurement of the beam profile. Figure 5 shows QCL beam profiles before and after 10 cm of propagation through the HW. Under optimal coupling conditions, Fig. 5 shows that the HW has a spatial mode cleansing effect which favors TEM_{00} propagation while filtering out higher order mode contributions which are detrimental to heterodyne mixing efficiency. Power measurements indicated that the power coupling efficiency was ~9% below the theoretical limit.

#143438 - $15.00 USD Received 1 Mar 2011; revised 6 Apr 2011; accepted 19 Apr 2011; published 25 Apr 2011

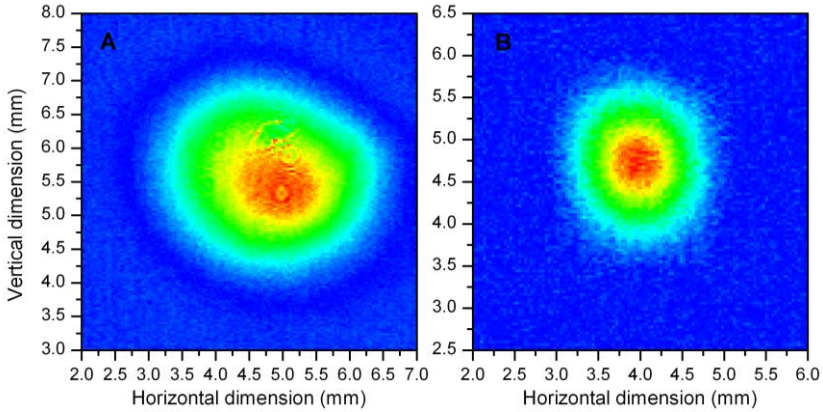

Fig. 5. Far field Quantum cascade laser beam contour at the input (A) and output (B) of the hollow waveguide mixing circuit.

In addition to the higher order mode cleansing effect, the HW was also observed to strongly reduce optical feedback effects, primarily from the detector. As spurious light does not match the stringent back-coupling conditions, it tends to excite higher order modes that are further attenuated.

3.2 Blackbody radiation coupling

The incoherent radiation input sub-module includes a reference blackbody source whose temperature can be adjusted from 263 to 823 K. A sample cell can be introduced in the beam-path of the blackbody radiation. A second blackbody operating either at 80K or at ambient temperature provides the radiometric reference against which the input incoherent radiation is measured. As the blackbody is an extended source, the input coupling conditions to the HW are rather relaxed. The incoherent radiation coupling was also checked using the infrared camera but in the near field due to the low brightness of the source.

4. Laser heterodyne spectro-radiometry

Before performing heterodyne spectro-radiometry with the HW-based system, the two photomixers were characterized in terms of optimum LO power [23] and temporal stability of heterodyne signals. Both detectors are subsequently used to record heterodyne spectra of carbonyl sulfide.

4.1 Liquid nitrogen and thermoelectrically cooled photomixer comparison

The LN_2 cooled detector is a 100x100 μm square photodiode, including a resonant optical cavity to maximize the bandwidth. The heterodyne efficiency was measured to be 0.46. To establish the optimum LO power level on the photomixer, a wire grid polarizer is inserted into the optical path, just after the QCL collimation lens, and rotated to adjust the transmitted laser power. Figure 6 A shows both the heterodyne signal to noise ratio (SNR - black data points) and the heterodyne signal (blue data points) as a function of the LO power.

As the LO power increases from zero the heterodyne signal and the SNR increase accordingly. The SNR reaches a maximum for a LO power of 150 μW. Further increases in LO power result in reduced SNR because of reduced responsivity of the detector due to saturation effects [23]. Operating at the optimum LO power level has the additional benefit of reducing the dependence of the heterodyne SNR on the LO power level (horizontal tangent).

The temporal stability was measured through Allan variance analysis [24]. Figure 6 B shows plots for both the heterodyne signal and the DC component of the detector's signal. Compared to previous measurements [12] obtained on a similar instrument using a free space mixing configuration, temporal stability of the heterodyne signal is increased by one order of magnitude. Slow drifts, which become significant after 300s of operation, may be due to

#143438 - $15.00 USD Received 1 Mar 2011; revised 6 Apr 2011; accepted 19 Apr 2011; published 25 Apr 2011

ambient temperature variations or LO drifts. The rollover point of the DC signal appears earlier (~30s), and is related to dark current fluctuations since the roll over point is unaffected by the laser being on or off. The LO stability is therefore at least better than 30s.

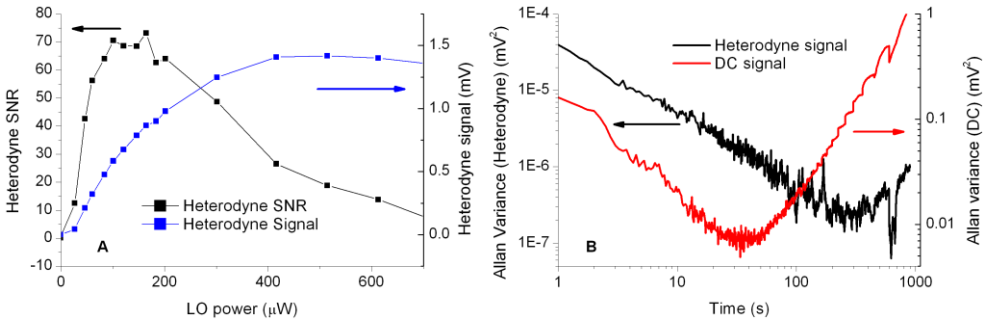

Fig. 6. Measurements with the LN_2 cooled photomixer. The bandwidth was 400 MHz, the blackbody temperature was 573 K and the integration time was 50 ms. A) evolution of the heterodyne signal to noise ratio (black data points and left Y axis) and the heterodyne signal (blue data points and right Y axis) as the LO power is varied. B) Allan variance plots of the heterodyne signal (left axis) and the DC signal (right Y axis).

An alternate photodetector was also considered and evaluated with the HW-based LHSR. The core element of this photomixer is composed of a HgCdZnTe circular photodiode with a 20 µm active area. (PVI, VIGO Systems). A hyperhemispherical lens in which the detector is immersed increases the effective detector size to 100 µm. The detector is actively controlled in temperature by a multi-stage Peltier element and operates at –60°C. It is reverse biased to increase the bandwidth and impedance-matched to a transimpedance amplifier. The heterodyne efficiency is not known, and was assumed to be at a higher limit of 0.5.

Heterodyne signals versus LO power are shown in Fig. 7 A. The optimum LO power for the TEC mixer is 200 µW. The roll-over of the heterodyne signal is more pronounced than in the case of the LN_2 cooled photomixer, and may be related to the 20 times higher optical power density received by the detector chip.

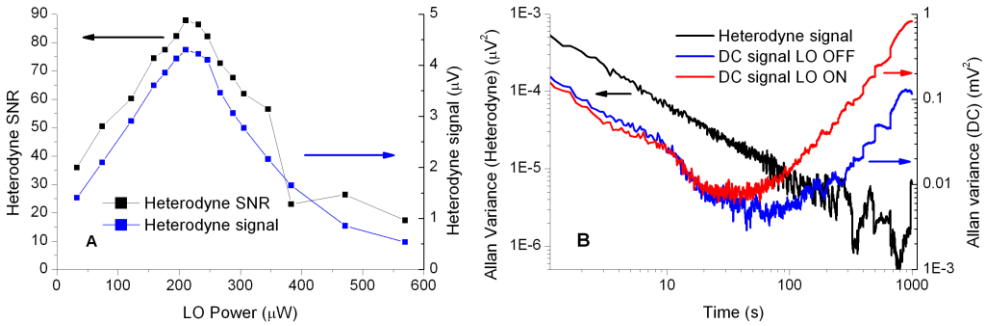

Fig. 7. Measurements with the TEC photomixer. The bandwidth was 600 MHz, the blackbody temperature was 823K and the integration time was 50 ms. A) evolution of the heterodyne signal to noise ratio (black data points, left Y axis) and the heterodyne signal (blue data points, right Y axis) as the LO power is varied. B) Allan variance plots of the heterodyne signal (left axis) and the DC signal (right Y axis).

Temporal stability was measured to be higher than for the LN_2 photomixer, as shown in Fig. 7 B. The record was stopped after 1000 seconds while the signal was still following white noise behaviour.

As in Fig. 6, the Allan variance of the detector DC signal shown in Fig. 7, exhibits a earlier roll-over point compared to that of the heterodyne signal. As the roll-over point is almost unaffected whether the LO beam illuminates the detector or not, the limits can be traced to drifts in the dark current.

#143438 - $15.00 USD Received 1 Mar 2011; revised 6 Apr 2011; accepted 19 Apr 2011; published 25 Apr 2011

4.2 Heterodyne spectro-radiometry

Following the determination of the optimum LO power, the heterodyne detection perfomance of the HW mixing circuit has been investigated using both detectors. A figure of merit parameter ρ, defined as the ratio of the measured detection limit with that of an ideal shot noise limited instrument, is expressed as:

$$\rho = \frac{\eta \cdot \Delta \cdot \sqrt{B \cdot \tau}}{\exp\left(\frac{h\nu}{kT}\right) - 1} \cdot \frac{1}{SNR_m}, \tag{3}$$

where η is the heterodyne efficiency, Δ the transmission of the incoherent radiation sub-module, B the double sideband bandwidth, τ the integration time, T the background blackbody temperature, and SNR_m, the measured signal to noise ratio from the data. Table 1 summarizes the measured performance of the instrument, expressed using the ρ parameter, for a range of experimental conditions including different resolutions, integration times and background blackbody temperatures.

Table 1. Summary of the performance of the hollow waveguide LHSR using both LN_2 and TEC photomixers under a variety of operating conditions.

Mixer	LO Power (μW)	Temp (K)	B (MHz)	Center (MHz)	τ (ms)	η	SNR	ρ
LN_2	150	573	400	700	50	0.46	73	1.78
LN_2	100 to 180	573	400	700	500	0.46	233	1.72
LN_2	100 to 180	573	400	700	50	0.46	63	2.01
TEC	200	823	600	700	50	0.50	88	4.79
TEC	140 to 220	573	400	700	500	0.50	56	7.77
TEC	140 to 220	573	400	700	50	0.50	17	8.09
TEC	130 to 290	573	600	450	500	0.50	80	6.66
TEC	130 to 290	573	600	450	50	0.50	30	5.62

During these investigations, the LN_2 photomixer consistently performed within a factor of two of the ultimate heterodyne shot noise limit. The previous version of the LHSR instrument [12] operated three times above the shot noise limit in fixed LO frequency mode and about ten times in LO scanning mode. The improvements brought about by the use of the HW mixing circuit are significant, as the noise performance is consistently reproducible at a single wavelength and is maintained during wavelength scans. Although the consistency of performance from the TEC photomixer was lower, with the best operation achieved within five times the shot noise limit, this is nevertheless an unprecedented result for a LHSR operating with no cryogenically cooled components. Furthermore, calculations of TEC photomixer performance are made with the assumption of a 50% heterodyne efficiency, since no information was available from the manufacturer. Therefore, confidence in the ρ parameter is lower than in the LN_2 case. However, in practice, heterodyne efficiencies higher than 50% are uncommon, and the calculated ρ parameter represents a worst case scenario (a lower heterodyne efficiency would mean that the ρ parameters are over-estimated). The values given in Table 1 also suggest that performance optimization is possible by selection of the appropriate RF filter; using a band-pass filter centered at lower frequency (450 MHz versus 700 MHz) where the detector response is higher leads to enhanced performance.

#143438 - $15.00 USD Received 1 Mar 2011; revised 6 Apr 2011; accepted 19 Apr 2011; published 25 Apr 2011

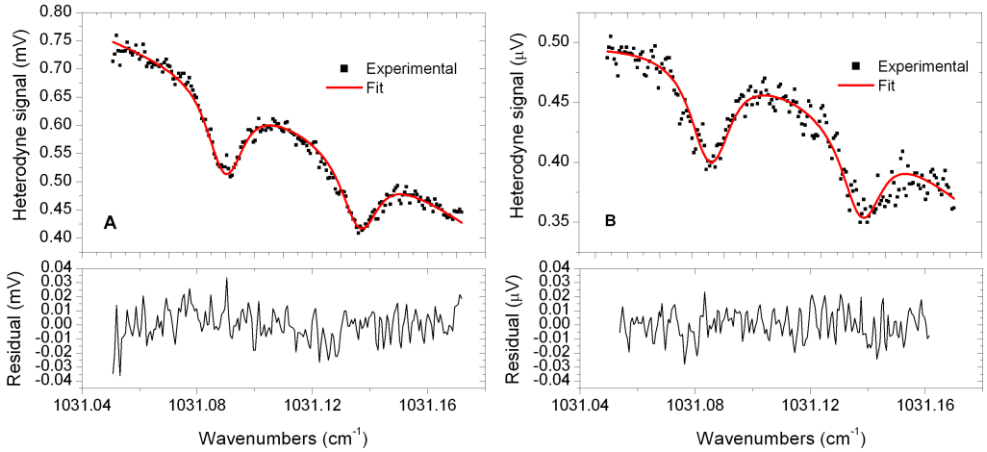

Fig. 8. Measured and fitted calculated heterodyne absorption spectra of carbonyl sulphide and associated residuals. A) spectrum was recorded with the LN_2 photomixer, and B) spectrum recorded with the TEC photomixer. The black dots are the measured spectra obtained with a 5 cm long gas cell containing 29 Torr of OCS, while the red curve shows a fitted calculated spectrum. The lower panels show the corresponding residuals. The blackbody temperature was 573 K, double side band detection bandwidth was 400 MHz with an integration time of 500 ms and the LO power was 150 μW.

To perform molecular spectro-radiometry with the instrument, a 5 cm long gas cell filled with 29 Torr of carbonyl sulphide (OCS) was placed in the beam path between the blackbody source and the HW mixing circuit (see Fig. 4). Carbonyl sulphide possesses strong fundamental ro-vibrational transitions coinciding with the QCL tuning range and was therefore an excellent test sample.

The local oscillator was tuned by modulating the applied current with a sawtooth waveform produced by a function generator. Scan parameters were optimized to allow full spectral coverage of the chosen spectral line of OCS; typical scans covered 3 to 4 GHz with sweep times ranging from 20 to 1000 s. An electronic bandpass filter centred at 700 MHz with a pass band of 200 MHz set the double sideband detection bandwidth to 400 MHz. In absorption mode the background blackbody temperature was set at 573 K, providing a hot background susceptible to absorption by the OCS molecules contained in the gas cell. Measurements were made using both the LN_2 and TEC cooled photomixers on the P42 transition of the $2\nu_2$ OCS band located at 1031.1095 cm^{-1} with a line strength of 2.58×10^{-21} $cm^{-1}/(molec.cm^{-2})$. Figure 8 shows heterodyne absorption spectra of OCS; the black dots correspond to the experimentally measured heterodyne signal while the solid red curve is the calculation based on a model of the instrument. The bottom panels show the residuals.

The model includes a line-by-line spectroscopic algorithm and an idealized top-hat instrument line shape function corresponding to the RF filter response. The doublet structure of the observed spectrum (rather than a single absorption line) is a consequence of the instrument line shape: each line in Fig. 8 is the same OCS transition measured in the upper and lower 200 MHz sideband as described in ref. 12 and 13. The model also includes a quadratic baseline as well as two parameters for absolute and relative frequency correction.

Generally, the relative quality of the spectra obtained with the LN_2 and TEC photomixers confirms the previously derived values of the ρ parameter, given in Table 1. The heterodyne detection performance of the TEC photomixer is approximately two to three times worse than that of the LN_2 device. However, this remains an impressive result given that the TEC mixer does not require cryogenic cooling and exhibits superior levels of temporal stability. Previous attempts to obtain heterodyne spectra with the TEC photomixer using "conventional free-space" beam-mixing have been unsuccessful. The immersed lens of the detector, which is a fast optic, tightens the tolerances placed on optical alignment constraints and increases the wavefront distortions and errors. The use of the hollow waveguide provides a way to

#143438 - $15.00 USD Received 1 Mar 2011; revised 6 Apr 2011; accepted 19 Apr 2011; published 25 Apr 2011

overcome alignment issues by ensuring perfect spatial mode coincidence, and thus enables high-quality photomixing with TEC devices.

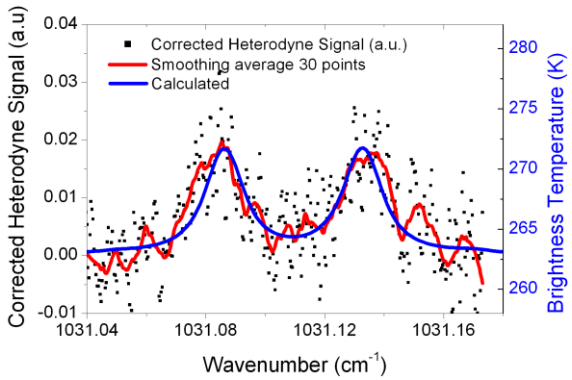

Fig. 9. Heterodyne emission spectrum of OCS (29 Torr, 5 cm). The black dots are the raw experimental measurements corrected for baseline effects, the red curve is a 30-point smoothed average. The blue trace is the theoretical calculation of the brightness temperature.

Heterodyne measurements of OCS emission were made using the LN_2 photomixer. In emission mode the hot blackbody was replaced by a blackbody operating below room temperature (263 K) to provide contrast against the intrinsic molecular emission of the OCS. Figure 9 shows the results obtained in emission mode, using a 400 MHz bandwidth (double side band) with a two second integration time. The LO power varied between 50 and 100 μW over the spectral range due to current modulation.

The emission spectrum is far noisier than the absorption spectra presented earlier. This is expected due to the cold background and the relatively low level of emission from the gas compared to the blackbody. Despite the noise, the smoothed average exhibits an unambiguous emission signature which is consistent with the simulated spectrum. The amplitude of the emission corresponds to a 5 K brightness temperature difference, which corresponds to a source radiance variation of 1 $\mu W/cm^2.st.cm^{-1}$, or, given the resolution and the narrow field of view, to a total received power variation of 12 femtowatts. As the SNR of the black dot signal approaches one, these figures provide experimental estimates of the instrument detection limit for a 2 second integration time.

5. Conclusion and outlook

The use and advantages of hollow waveguide technology for heterodyne spectro-radiometry have been studied. This has been done through the development of a hollow waveguide mixing module, its efficient coupling with quantum cascade lasers, and the laboratory demonstration of high-quality heterodyne spectro-radiometry on carbonyl sulphide. The following advantages were observed compared with a conventional free-space implementation of the coherent mixing circuit:

- Propagation of radiation through the hollow waveguide favors the fundamental laser spatial mode. It effectively provided spatial mode cleansing which promotes higher optical mixing efficiency.
- The waveguide also ensures optimum co-propagation and phase front alignment of the LO and incoherent radiation. Therefore the time consuming process of beam co-alignment on a traditional “free-space” heterodyne system has been eliminated.
- One order of magnitude improvement in temporal stability has been measured. With a peltier-cooled actively temperature controlled detector, the stability was enhanced by more than two orders of magnitude.

#143438 - $15.00 USD Received 1 Mar 2011; revised 6 Apr 2011; accepted 19 Apr 2011; published 25 Apr 2011

- Routine heterodyne operation within a factor of two of the fundamental shot noise limit was achieved.
- The first high-quality radiometric heterodyne measurements were made using a thermoelectrically cooled detector. Performance was demonstrated to be within five times of the shot noise limit. This result opens the way for LHSR systems without the need for cryogenic cooling.

The successful demonstration and performance assessment of optical photomixing based on hollow waveguide architecture was a prerequisite before undertaking development of a fully integrated LHSR. Using a hollow waveguide for optical mixing supersedes the traditional "free-space" optical way and therefore future work will include the development of a fully optically integrated instrument.

Acknowledgements

The authors wish to thank Wayne Robins from the Precision Development Facility of the Space Science & Technology Department for his work in precision mechanical engineering. Gary Williams is acknowledged for his continuous technical support. This work was supported by the Centre for Earth Observation Instrumentation established by the UK Natural Environment Research Council (NERC) and the Technology Strategy Board (TSB). Support from the NERC research grant number NE/H002383/1 is also acknowledged.

#143438 - $15.00 USD Received 1 Mar 2011; revised 6 Apr 2011; accepted 19 Apr 2011; published 25 Apr 2011